Research paper

Block Copolymer Crosslinked Nanoassemblies Co-entrapping Acridine Yellow and Doxorubicin for Cancer Theranostics

Pengxiao Cao, Andrei Ponta, JiAe Kim, Younsoo Bae*

Department of Pharmaceutical Sciences, College of Pharmacy, University of Kentucky, 789 South Limestone, Lexington, KY 40536, USA

ABSTRACT

Aims: To develop block copolymer crosslinked nanoassemblies (CNAs) that co-entrap an imaging dye (Acridine Yellow: AY) and therapeutic agent (doxorubicin: DOX) as novel nanoparticle drug carriers for a combined application of drug delivery-based therapy and diagnostic imaging technologies (theranostics).
Methodology: The AY-crosslinked CNAs (CNAs) were synthesized from biocompatible poly(ethylene glycol)-poly(aspartate) block copolymers by using AY as a crosslinker while DOX was physically entrapped in the particle through an ionic interaction. AY-CNAs and AY-CNAs with DOX were characterized to determine their particle properties (molecular weight, size, and optical properties), intracellular uptake and cytotoxicity in an in vitro cell culture system using human colon HT29 and lung A549 cancer cell lines, and tissue accumulation and tumor-preferential drug delivery efficiency ex vivo with a xenograft mouse tumor model.
Results: AY-CNAs appeared to maintain nanoscale particle sizes (< 20 nm), fluorescence optical properties, and negative surface charge before and after drug entrapment. AY-CNAs with DOX were confirmed to kill cancer cells as effectively as free drug formulations, and to enhance intracellular uptake in vitro and tumor accumulation ex vivo.
Conclusion: These results demonstrate that block copolymer nanoassemblies crosslinked with an imaging dye are promising platforms for the development of theranostic nanoparticle drug carriers.

Keywords: Nanoparticles, nanoassemblies, drug carriers, drug delivery, imaging, theranostics

1. INTRODUCTION

Nanoparticles have drawn attention as promising tools that can combine therapeutic and diagnostic modalities, which may allow doctors to monitor a progress of treatment and determine an optimal dose and timely intervention [1, 2]. Such a combination of therapy and diagnosis of disease, often known as theranostics, is particularly beneficial for treating cancer patients who respond to chemotherapy differently [3, 4]. An optimal dose of an anticancer drug is typically determined by balancing chemotherapeutic efficacy and toxicity based on pharmacokinetic profiles of the drug [5, 6]. Nanoparticle drug carriers for theranostics are expected to expedite this dosing regimen determination process and provide novel cancer chemotherapy with enhanced efficacy and reduced toxicity [7, 8].

In recent years, various types of nanoparticles have been developed for cancer theranostics by conjugating imaging agents on the surface and entrapping therapeutic agents in the core [9, 10]. This approach is widely used for labeling proteins, RNAs, and DNA in biology, but often dramatically changes the particle properties of nanoparticles such as particle size, shape, surface charge, and interactions with live cells [11, 12]. One of the methods to avoid these undesirable particle property changes is to entrap imaging dyes in the core of nanoparticles [13]. However, entrapping imaging dyes into nanoparticles may lead to other issues such as fluorescence quenching, dye spectrum shifting, or reduced drug loading [14, 15]. Therefore, developing a novel method that can entrap imaging agents in the nanoparticle core without altering particle properties is critically important for successful theranostics.

In addition to an imaging dye, a therapeutic agent is another payload to which careful consideration needs to be paid for the development of theranostic nanoparticles [16, 17]. Drug molecules are generally entrapped in nanoparticles through either physical entrapment or chemical conjugation [18]. Although chemical drug conjugation via a degradable linker is advantageous to avoid uncontrolled release of drug from nanoparticle drug carriers, it frequently requires complicated chemistry for the synthesis of prodrugs and linkers [19-21]. The chemical drug conjugation approach also requires validation if nanoparticles release the drug in its active form without forming byproduct during a linker degradation process. In this regard, physical drug entrapment is a more viable option to develop theranostic nanoparticles for combination delivery of imaging and therapeutic agents. Hydrophobic and ionic interactions are often used alone or in combination to entrap anticancer drugs inside nanoparticles. One of the model anticancer drugs used widely in drug delivery study is doxorubicin (DOX), an anthracycline agent that is effective to kill various types of cancer cells in the clinic [22]. The anthracycline portion of DOX is responsible for DNA intercalation and hydrophobic interaction with other molecules in the body while the amino group of DOX on the 4’ position of the sugar can be used for ionic binding. DOX also has autofluorescence that can be easily monitored by UV-VIS and fluorescence spectrometry.

We have been developing biocompatible block copolymer crosslinked nanoassemblies (CNAs) for drug delivery and imaging [23, 24]. In this study, we used CNAs as molecular platforms to develop novel theranostic carriers for combination delivery of an imaging dye (Acridine Yellow: AY) and anticancer drug (DOX). As illustrated in Figure 1, AY was used as a crosslinker while DOX was entrapped in CNAs through an ionic interaction. The AY-crosslinked CNAs (AY-CNAs) were prepared from poly(ethylene glycol)-poly(aspartate) block copolymers that provide carboxyl groups for crosslinking and drug binding in the core enveloped by a hydrophilic shell. With this development approach, nanoparticles that co-entrap imaging and therapeutic agents can be prepared without any complicated chemical modification. The objective of this study is to characterize optical properties, intracellular uptake profile, and tissue accumulation patterns of AY-CNAs in vitro and ex vivo. These results are expected to provide valuable insights into the development of theranostic nanoparticles for cancer treatment by combining bioimaging and drug delivery technologies.

2. MATERIAL AND METHODS

2.1 Materials

NOF corporation (Japan) provided α-methoxy-ω-amino poly(ethylene glycol) (PEG) (MW = 5,000). Doxorubicin hydrochloride (DOX-HCl), anhydrous triphosgene, L-aspartic acid β-benzyl ester, N,N'-Diisopropylcarbodiimide (DIC), N-Hydroxysuccinimide (NHS), 4-Dimethylaminopyridine (DMAP), ethyl ether, dimethyl sulfoxide (DMSO), and other solvents were purchased from Sigma-Aldrich (USA). Acridine yellow (AY), cellulose dialysis bags with

6-8 kDa molecular weight cut off (MWCO), Slide-A-Lyzer dialysis cassettes with 10 kDa MWCO, sterile filters (0.22 µm), and matrigel were purchased from Fisher Scientific (USA). Human colon (HT29) and lung (A549) cancer cell lines, and cell culture media (McCoy's 5A and F-12K) were purchased from ATCC (USA). Millicell EZ slide with 8 chambers were obtained from EMD Millipore (USA).

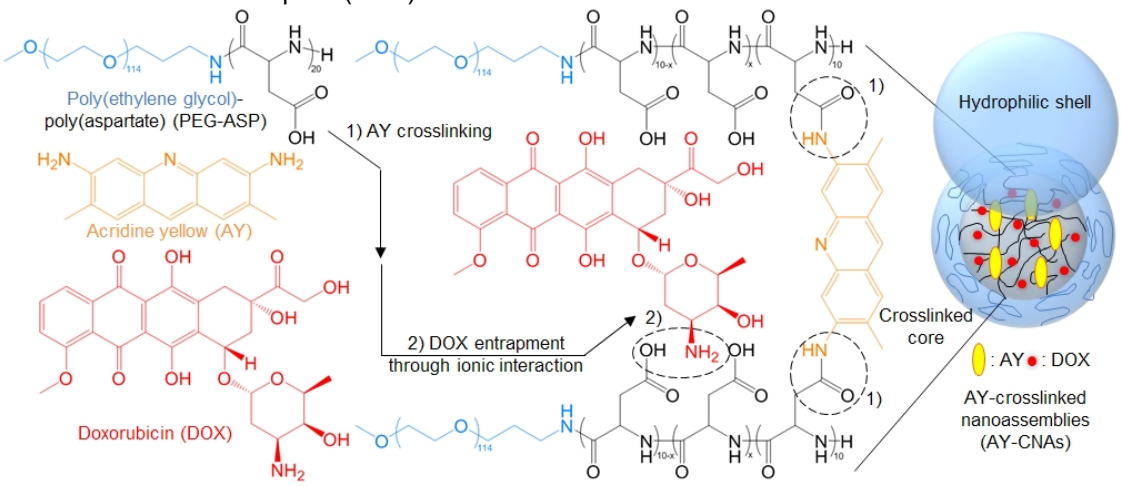

Fig. 1. Synthesis of AY-CNAs

2.2 Synthesis of AY-CNAs

Figure 1 shows the synthesis protocol of AY-CNAs entrapping DOX. PEG-ASP was synthesized as described elsewhere [18, 25, 26]. L-aspartic acid β-benzyl ester was reacted with triphosgene to obtain β-benzyl aspartate N-carboxyanhydride (BLA-NCA) monomers. BLA-NCA was polymerized by using PEG as a macroinitiator for 2 days in DMSO (50 mg/mL, 40°C, nitrogen atmosphere). The polymerization produced PEG-poly(β-benzyl L-aspartate) (PEG-BLA), comprising 5 kDa PEG and 20 repeating units of ASP groups. The benzyl ester protecting groups were removed in a 0.1 N NaOH solution to obtain PEG-ASP. Excess NaOH was removed from the polymer solution by dialysis, followed by freeze drying of PEG-ASP. The purified PEG-ASP was reacted with AY by adjusting the molar ratio between the aspartate groups of PEG-ASP and amino groups of AY (2:1) for a 50% crosslinking yield. PEG-ASP and AY were dissolved in DMSO in the presence of DIC, NHS, and DMAP for three days at room temperature with gentle stirring. The product, AY-CNAs, was precipitated in ethyl ether, dialyzed against deionized water, and collected by freeze drying. AY-CNAs were further purified by gel separation using a Sephadex G25 column, and unreacted AY was removed completely from AY-CNAs. A single band on the column containing AY-CNAs was collected, dialyzed against deionized water, and freeze dried. DOX was entrapped in AY-CNAs in deionized water through the ionic interaction between the amino group of DOX and carboxyl groups of AY-CNAs, following the method previously reported. Empty AY-CNAs and AY-CNAs with DOX were stored at -20°C for future use.

2.3 Characterization of AY-CNAs

The molecular weight and its distribution of AY-CNAs were analyzed by gel permeation chromatography (GPC), using Shimadzu LC20 system equipped with a GPC analysis module. The particle size and surface charge of AY-CNAs and AY-CNAs with DOX were determined by a Zetasizer Nano ZS (Malvern, UK), an instrument capable of measuring dynamic light scattering (DLS) and zeta potential of nanoparticles in aqueous solutions. The amount of DOX entrapped in AY-CNAs was quantified by fluorescence spectrometry while empty AY-CNAs were used as blanks.

2.4 Cellular uptake observations

Time-dependent changes in cellular uptake of AY-CNAs were monitored in a human colon HT29 cancer cell line in vitro by using a fluorescence microscope (EVOS, Advanced Microscopy Group, USA). Cells were cultured in McCoy's 5A media containing 10% FBS at 37°C in a humidified atmosphere with 5% CO_2. For cellular uptake study, cells were seeded in 8 chamber slides (1×10^4 cells/chamber) and allowed to attach on the bottom of the slides overnight. The cells were then treated with 100 µg/mL AY-CNAs for 24 h. The sample-containing media were removed at 5 min, 0.5 h, 3 h, and 24 h, and the cells were washed with PBS three times. Cell nuclei were stained with a Hoechst dye prior to fluorescence microscopy. Cell images were taken through separate light channels for a bright field, Hoechst, and AY, and processed using software ImageJ (National Institutes of Health, USA). In separate experiments, cells treated with AY-CNAs in each chamber were dissolved in 80% DMSO, and the fluorescence intensity of AY-CNAs in the cell lysates were quantified by fluorescence spectrometry. The intracellular concentrations of AY-CNAs were normalized with respect to the initial concentration of AY-CNAs (100 µg/mL) in each well. Data were obtained from triplicate experiments.

2.5 Drug release evaluation

Release of DOX from AY-CNAs was tested by the dialysis method under a sink condition at pH 7.4, 37°C. Ten milligrams of AY-CNAs with DOX were dissolved in 3 mL PBS, and the solution was put in dialysis cassettes (MWCO 10 kDa). The dialysis cassettes (n = 3) were stored in a preheated stainless steel bin containing 5 L PBS. The samples were dialyzed for 48 h, and 50 µL of the solution in each dialysis cassette was collected at 0.5, 1, 3, 6, 24, and 48 h. DOX released was quantified by fluorescence spectrometry as described above.

2.6 In vitro cytotoxicity assay

Cytotoxicity of AY-CNAs with DOX was evaluated in an in vitro cell culture system by using HT29 and A549 cell lines. HT29 and A549 cells were cultured in McCoy's 5A and F12K media, respectively, containing 10% FBS at 37°C in a humidified atmosphere with 5% CO_2. Cells were seeded in a 96 well plate (5×10^3 cells/well). After 24 h, the cells were treated with free DOX or AY-CNAs with DOX at various concentrations (normalized with respect to DOX). Empty AY-CNAs were used as controls. Cell viability was determined at 72 h post treatment by using a resazurin assay, which measures metabolic activity of mitochondria in live cells. The half maximal inhibitory concentration (IC50) of each sample was determined from the dose response curves by using GraphPad Prism software. The one-way analysis of variance (ANOVA) was used to determine statistical differences between means ($p < 0.05$).

2.7 Ex vivo imaging

Six-week old female SCID mice were obtained from Taconic (USA), and acclimated for a week on a regular diet. A xenograft mouse tumor model was prepared by injecting HT29 cells (3×10^6 cells) subcutaneously in the right flank of an animal. When the tumor volume surpassed 100 mm^3, AY-CNAs and AY-CNAs with DOX were injected into the tumor-bearing mice at 100 mg/kg through the tail vein. Animals were euthanized at 0.5, 2, 6, and 24 h post injections. Tumors and other major organs (lung, heart, liver, spleen, kidney, small intestine, and brain) were collected at each time point. An in vivo imaging system (IVIS) was used to take ex vivo images of the harvested tissues with excitation at 465 nm and emission at 540 nm, based on the fluorescence spectra of free AY and DOX. The imaging condition was fixed to compare fluorescence intensities from the organ and tumor tissues.

3. RESULTS

3.1 Synthesis of AY-CNAs

Gel permeation chromatography (GPC) analysis in Figure 2 shows the successful synthesis of AY-CNAs. The molecular weight of PEG-ASP (7,300 kDa) increased as the crosslinking reaction proceeded as shown in the black line. Raw AY-CNAs included small molecule impurities that appeared after the PEG-ASP peak at around 27 minutes. After purification, AY-CNAs showed a single peak with a narrow molecular weight distribution (262,500 kDa, PDI = 1.18), which was within the size exclusion limit of our GPC (970 - 478,000 kDa). The molecular weight of AY-CNAs indicates that a single CNA particle consists of 31 - 36 PEG-ASP chains depending on the crosslinking yield. Our attempt to determine the exact crosslinking yield was unsuccessful due to peak overlapping on proton nuclear magnetic resonance, and fluorescence spectrometry was used to quantify AY-CNAs by measuring AY. As shown in Figure 3, maximum emission wavelengths for AY and DOX were distinguishable by adjusting the excitation wavelength up to 500 nm. These optical properties of AY and DOX were initially thought to be useful quantifying a combine signal of AY and DOX. However, to avoid an overlapping signal between AY and DOX, we decided to used AY-CNAs and AY-CNAs with DOX for following experiments. Table 1 summarizes characterization data. The particle size of AY-CNAs was 15.7 ± 5.3 nm, and the polydispersity index (PDI) was 0.384. The zeta potential of AY-CNAs was -14.7 ± 9.8 mV, indicating that the particle may be too small for the PEG shell to completely shield the charge of the negatively charged core. The particle size of AY-CNAs was similar after entrapping DOX while the PDI went up to 0.418. The amount of DOX loaded in AY-CNAs was 4.65% by weight, which was significantly lower than other previous CNAs. The surface charge of AY-CNAs remained negatively charged (-10.2 ± 6.2 mV) after entrapping DOX.

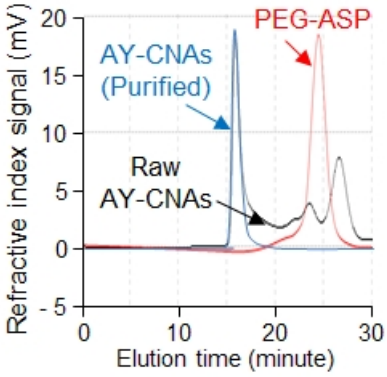

Fig. 2. Gel permeation chromatography analysis

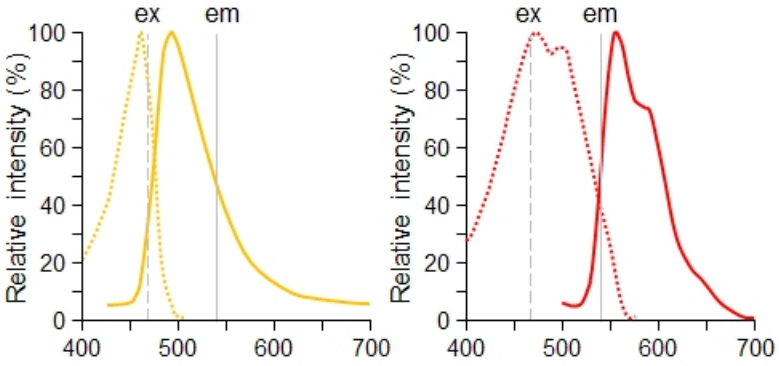

Fig. 3. Fluorescence spectra of AY and DOX

Table 1. Characterization data summary

	Particle size (nm)	PDI	Zeta potential (mV)	DOX loading (weight %)
AY-CNAs	15.69 ± 5.33	0.384	- 14.70 ± 9.78	N.A.
AY-CNAs with DOX	18.17 ± 5.98	0.418	- 10.20 ± 6.24	4.65

3.2 Intracellular uptake profile

Figure 4 shows time-dependent changes in intracellular uptake of AY-CNAs in HT29 cells. Non-specific binding to the cellular membrane was not observed between AY-CNAs and HT29 cells in 5 minutes. However, AY-CNAs entered and spread in the cytoplasm in 30 minutes. Interestingly, some AY-CNAs were confirmed to migrate into the cell nuclei as indicated in the merged image in green. No further change was observed after 24 h following a gradual increase in fluorescence intensity of AY-CNAs between 3 and 24 h. The intracellular concentration of AY-CNAs was also quantified from cell lysates in separate experiments. As shown in Figure 5, intracellular uptake of AY-CNAs followed biphasic kinetics, which involves a fast uptake in the early stage (up to 6 h) and a slow internalization into the cell in the late stage. The intracellular concentration of AY-CNAs did not equilibrate to the particle concentration in the media (100 μg/mL) under our experimental conditions.

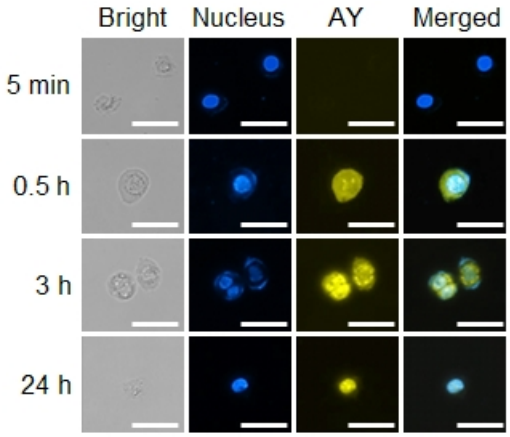

Fig. 4. Intracellular uptake of AY-CNAs. Bright field (40X magnification), Hoechst-stained nucleus (blue), AY (yellow), and merged images of HT29 cells (bar = 50 μm).

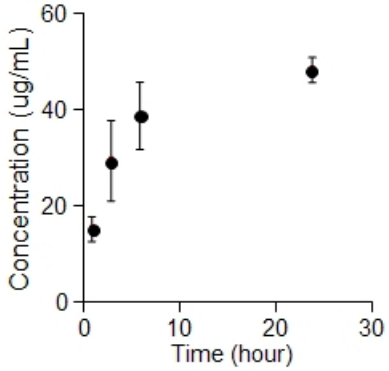

Fig. 5. A time-dependent change in concentration of AY-CNAs in HT29 cells.

3.3 Drug release patterns

Release of DOX was monitored for 48 h in the physiological condition (37°C and pH 7.4) as shown in Figure 6. AY-CNAs released more than 50% of DOX in 1 h, yet they slowed drug release for the next 48 h. Approximately 20% of total DOX entrapped in AY-CNAs was released between 3-48 h, although the drug release half-life was 1.34 h by curve fitting. Based on both intracellular uptake and drug release patterns, these results suggest that the amount of DOX that AY-CNAs can transport inside the HT29 cells would be approximately 12 - 17 % (= DOX remaining × intracellular uptake yield) over the 48 h period. The effect of such a fast drug release and relatively low intracellular drug transport on anticancer efficacy was investigated subsequently in the cytotoxicity assays.

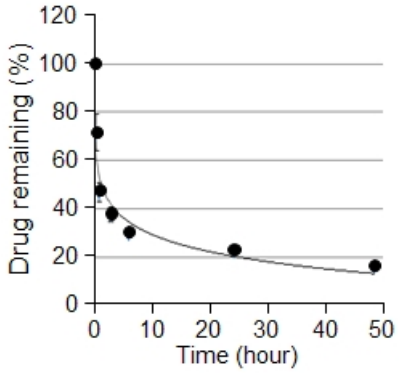

Fig. 6. DOX release from AY-CNAs (pH 7.4, 37°C, n = 3)

3.4 In vitro cytotoxicity of AY-CNAs with DOX

Cytotoxicity of AY-CNAs with DOX was evaluated in exponentially growing HT29 cells in vitro. A549 was used as an additional cancer cell line for the assay. As shown in Figure 7, sigmoidal dose-response curves were obtained from both cancer cell lines, following the treatment of the cells with AY-CNAs entrapping DOX. Table 2 summarizes the IC50 values of AY-CNAs, which range between 3.03 - 4.80 μM. Although relative IC50 values suggested that AY-CNAs with DOX would be less potent than free DOX, statistical analysis of the data revealed that both cell lines were equally sensitive to free DOX ($p = 0.240$) and AY-CNAs with DOX ($p = 0.051$). Considering the slow drug release from AY-CNAs after 3 h post incubation, it is noticeable that free DOX and AY-CNAs with DOX showed no significant difference in killing HT29 ($p = 0.224$) and A549 ($p = 0.654$) cancer cells.

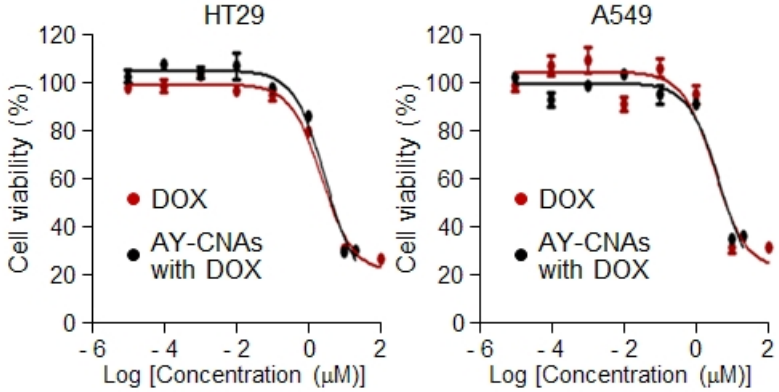

Fig. 7. Cytotoxicity of AY-CNAs against HT29 and A549 cells (triplicate assays, n = 8)

Table 2. In vitro cytotoxicity assays (triplicate assays, n = 8)

	IC50 (μM)		Relative IC50	
	HT29	A549	HT29	A549
DOX	2.44 ± 0.65	3.08 ± 0.47	1	1
AY-CNAs with DOX	3.03 ± 0.27	4.80 ± 1.09	1.56	1.24

3.5 Tissue distribution of AY-CNAs with DOX

Tissue accumulation patterns of AY-CNAs were investigated time-dependently as shown in Figure 8. The images were taken under the condition where AY and DOX showed equal fluorescence emission intensity at 540 nm with excitation at 465 nm as determined in Figure 3. In this way, signals from AY and DOX were obtained collectively. AY-CNAs appeared to accumulate in the kidneys, intestine, and tumors, while avoiding the uptake in the liver and spleen. The liver and spleen are two major organs of the mononuclear phagocyte system (MPS), which are responsible for removing foreign materials from the body. These results suggest that negatively charged AY-CNAs could be effective to suppress protein adsorption and cellular interactions in the body, yet they accumulated in the kidneys due to the relatively small particle size (< 20 nm). AY-CNAs with DOX also suppressed the hepatic and splenic uptake while accumulating in tumors. The images demonstrate that AY-CNAs with DOX increased signals in tumors in comparison to empty AY-CNAs presumably due to enhanced DOX accumulation in the tumors.

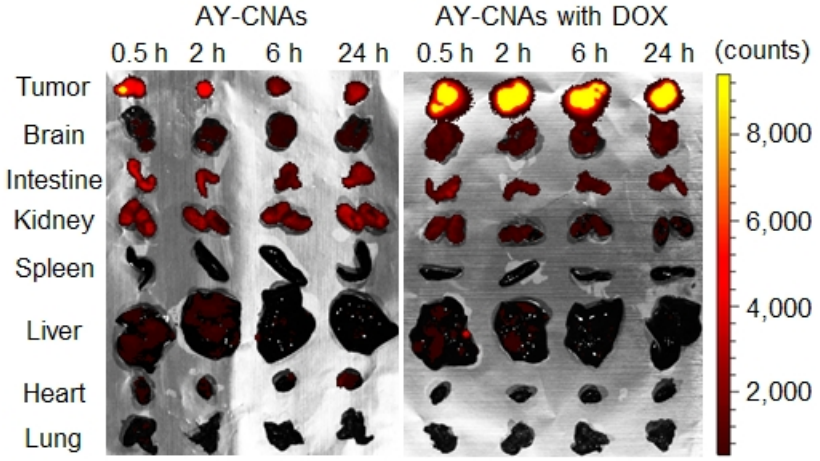

Fig. 8. Ex vivo imaging of tumors and major organs from mice received intravenously AY-CNAs and AY-CNAs with DOX.

4. DISCUSSION

AY-CNAs were synthesized by using AY as a crosslinker for conjugating PEG-ASP block copolymers. AY is also a fluorescent dye useful for in vitro and ex vivo imaging [27]. Nanoparticles for imaging are typically modified with fluorescent dyes on the surface. This modification method often alters particle properties of the nanoparticles, such as particle size, surface charge, biocompatibility, and pharmacokinetic profiles [28]. In comparison to this method, our approach to use a fluorescent dye as a crosslinker does not require additional chemical modification of a nanoparticle, and thus maintaining particle properties for optimal in vivo performance (prolonged blood circulation and minimum off-target accumulation).

AY-CNAs were uniform in terms of molecular weight distribution as shown in Table 1 and Figure 2. However, the particle size was relatively small (< 20 nm) as opposed to the CNAs we reported previously or other types of nanoparticles (50 - 100 nm in diameter). The small particle size suggested that the core of AY-CNAs could be tightly packed. Nanoparticles with a tightly packed core often induced a fluorescence quenching phenomenon, but AY-CNAs retained optical properties of AY and DOX as shown in Figures 3 and 4. Small particle size indeed compromised drug loading efficiency for the particles, and AY-CNAs showed less than 5 wt% of drug loading. Nevertheless, AY-CNAs with a small particle size seemed to enhance intracellular uptake of cancer cells. The particles successfully entered HT29 cancer cells as early as 30 minutes, and continue to accumulate in the cytoplasm and ultimately in the cell nucleus in 24 h (Figures 4 and 5). Such an efficient cell internalization pattern suggests that AY-CNAs would be a promising drug carrier for intracellular drug delivery. The mechanism by which AY-CNAs enter the cell certainly requires further study [29, 30].

Despite the promising properties (uniform particles with a small size and enhanced cell internalization capability), AY-CNAs released drug unexpectedly fast (Figure 6), demonstrating burst DOX release in 3 h and sustained release for the next 48 h. It is uncertain if such a biphasic drug release pattern would provide any benefit in terms of enhancing antitumor activity. Interestingly, fast release (or sustained release) did not affect cytotoxicity of AY-CNAs with DOX in an in vitro cell culture system. Both HT29 and A549 cells were sensitive to AY-CNAs with DOX, which were as effective as free DOX in terms of IC50 values (Figure 7). Ex vivo imaging suggest that sustained drug release from AY-CNAs in the late stage would still allow the particles to deliver drug to tumors and enhance drug concentrations in the tumor tissues preferentially, suppressing off-target drug distribution (Figure 8). It must be noted that AY-CNAs with a small particle size were confirmed to accumulate mainly in kidneys and intestine other than tumors. Pathological similarities among kidneys, intestine, and tumors have not been studied sufficiently yet, and the reason behind our findings remains uncertain. However, it is encouraging that AY-CNAs can be present in these tissues after 24 h, which might lead to the development of drug delivery systems for novel therapeutic or diagnostic applications.

5. CONCLUSION

In this study, AY-CNAs, block copolymer nanoassemblies crosslinked by a fluorescent dye, were synthesized for potential combination delivery of imaging and therapeutic agents to tumors. AY-CNAs were uniform in size and molecular weight distribution while maintaining negative surface charge before and after entrapping DOX, a model anticancer drug. Optical properties of AY and DOX were comparable yet different enough to distinguish, enabling both additive and differential quantifications of fluorescence emission signals at the same excitation wavelength. AY-CNAs entered cancer cells in 30 minutes post-incubation, and ultimately accumulated in cell nuclei in 24 h, presumably due to their small particle size (< 20 nm). AY-CNAs entrapping DOX released approximately 60% of the total drug entrapped in 3 h, and showed a sustained release of the remaining drug over the 48 period. Despite the biphasic drug release pattern, AY-CNAs with DOX showed cytotoxicity as effective as free DOX against human colon HT29 and lung A549 cancer cells in vitro. Ex vivo imaging results confirmed that AY-CNAs and AY-CNAs with DOX accumulate mainly in tumors and kidneys while suppressing hepatic and splenic uptake. Taken together, AY-CNAs are expected to be used as dual functional nanoscale carriers for bioimaging and drug delivery applications.

ACKNOWLEDGEMENTS

This research is supported by the Kentucky Lung Cancer Research Program.

REFERENCES

1. Lammers T, Aime S, Hennink WE, Storm G, Kiessling F. Theranostic nanomedicine. Acc Chem Res. 2011;44(10):1029-1038.
2. Chen W, Xu NF, Xu LG, Wang LB, Li ZK, Ma W, et al. Multifunctional Magnetoplasmonic Nanoparticle Assemblies for Cancer Therapy and Diagnostics (Theranostics). Macromol Rapid Comm. 2010;31(2):228-236.
3. Janib SM, Moses AS, MacKay JA. Imaging and drug delivery using theranostic nanoparticles. Adv Drug Deliver Rev. 2010;62(11):1052-1063.
4. Parveen S, Misra R, Sahoo SK. Nanoparticles: a boon to drug delivery, therapeutics, diagnostics and imaging. Nanomed-Nanotechnol. 2012;8(2):147-166.
5. Baselga J, Mita AC, Schoffski P, Dumez H, Rojo F, Tabernero J, et al. Using Pharmacokinetic and Pharmacodynamic Data in Early Decision Making Regarding Drug Development: A Phase I Clinical Trial Evaluating Tyrosine Kinase Inhibitor, AEE788. Clin Cancer Res. 2012;18(22):6364-6372.
6. Pagano A, Honore S, Esteve MA, Braguer D. Nanodrug potential in cancer therapy: efficacy/toxicity studies in cancer cells. Int J Nanotechnol. 2012;9(3-7):502-516.
7. Saif MW, Choma A, Salamone SJ, Chu E. Pharmacokinetically Guided Dose Adjustment of 5-Fluorouracil: A Rational Approach to Improving Therapeutic Outcomes. J Natl Cancer I. 2009;101(22):1543-1552.
8. Kopecek J. Biomaterials and Drug Delivery: Past, Present, and Future. Mol Pharm. 2010;7(4):922-925.
9. Xie J, Lee S, Chen XY. Nanoparticle-based theranostic agents. Adv Drug Deliver Rev. 2010;62(11):1064-1079.
10. Adair JH, Parette MP, Altinoglu EI, Kester M. Nanoparticulate Alternatives for Drug Delivery. Acs Nano. 2010;4(9):4967-4970.
11. Rosenblum LT, Kosaka N, Mitsunaga M, Choyke PL, Kobayashi H. In vivo molecular imaging using nanomaterials: General in vivo characteristics of nano-sized reagents and applications for cancer diagnosis (Review). Mol Membr Biol. 2010;27(7):274-285.
12. He CB, Hu YP, Yin LC, Tang C, Yin CH. Effects of particle size and surface charge on cellular uptake and biodistribution of polymeric nanoparticles. Biomaterials. 2010;31(13):3657-3666.
13. Cormode DP, Skajaa T, Fayad ZA, Mulder WJM. Nanotechnology in Medical Imaging Probe Design and Applications. Arterioscl Throm Vas. 2009;29(7):992-1000.
14. Louie AY. Multimodality Imaging Probes: Design and Challenges. Chem Rev. 2010;110(5):3146-3195.
15. Gao JH, Chen K, Luong R, Bouley DM, Mao H, Qiao TC, et al. A Novel Clinically Translatable Fluorescent Nanoparticle for Targeted Molecular Imaging of Tumors in Living Subjects. Nano Lett. 2012;12(1):281-286.
16. Yap TA, Sandhu SK, Workman P, de Bono JS. Envisioning the future of early anticancer drug development. Nat Rev Cancer. 2010;10(7):514-U525.
17. Rask-Andersen M, Almen MS, Schioth HB. Trends in the exploitation of novel drug targets. Nat Rev Drug Discov. 2011;10(8):579-590.
18. Lee HJ, Bae Y. Pharmaceutical Differences Between Block Copolymer Self-Assembled and Cross-Linked Nanoassemblies as Carriers for Tunable Drug Release. Pharm Res. 2013;30(2):478-488.
19. Larson N, Ghandehari H. Polymeric Conjugates for Drug Delivery. Chem Mater. 2012;24(5):840-853.
20. Binauld S, Stenzel MH. Acid-degradable polymers for drug delivery: a decade of innovation. Chem Commun. 2013;49(21):2082-2102.
21. Wanakule P, Roy K. Disease-Responsive Drug Delivery: The Next Generation of Smart Delivery Devices. Curr Drug Metab. 2012;13(1):42-49.

22. Bae Y, Kataoka K. Intelligent polymeric micelles from functional poly(ethylene glycol)-poly(amino acid) block copolymers. Adv Drug Deliver Rev. 2009;61(10):768-784.
23. Lee HJ, Bae Y. Cross-Linked Nanoassemblies from Poly(ethylene glycol)-poly(aspartate) Block Copolymers as Stable Supramolecular Templates for Particulate Drug Delivery. Biomacromolecules. 2011;12(7):2686-2696.
24. Lee HJ, Ponta A, Bae Y. Polymer nanoassemblies for cancer treatment and imaging. Ther Deliv. 2010;1(6):803-817.
25. Bae Y, Jang W-D, Nishiyama N, Fukushima S, Kataoka K. Multifunctional polymeric micelles with folate-mediated cancer cell targeting and pH-triggered drug releasing properties for active intracellular drug delivery. Mol BioSyst. 2005;1(3):242-250.
26. Bae Y, Fukushima S, Harada A, Kataoka K. Design of environment-sensitive supramolecular assemblies for intracellular drug delivery: Polymeric micelles that are responsive to intracellular pH change. Angew Chem Int Ed. 2003;42(38):4640-4643.
27. Mahmood T, Wu Y, Loriot D, Kuimova M, Ladame S. Closing the ring to bring up the light: synthesis of a hexacyclic acridinium cyanine dye. Chemistry. 2012;18(39):12349-12356.
28. Cho EC, Au L, Zhang Q, Xia YN. The Effects of Size, Shape, and Surface Functional Group of Gold Nanostructures on Their Adsorption and Internalization by Cells. Small. 2010;6(4):517-522.
29. Yoo JW, Doshi N, Mitragotri S. Endocytosis and Intracellular Distribution of PLGA Particles in Endothelial Cells: Effect of Particle Geometry. Macromol Rapid Comm. 2010;31(2):142-148.
30. Misra R, Sahoo SK. Intracellular trafficking of nuclear localization signal conjugated nanoparticles for cancer therapy. Eur J Pharm Sci. 2010;39(1-3):152-163.